

Hierarchical Policies for Cluttered-Scene Grasping with Latent Plans

Lirui Wang¹, Yu Xiang², Dieter Fox^{1,2}

¹University of Washington, ²NVIDIA

`liruiw@cs.washington.edu, {yux, dieterf}@nvidia.com`

Abstract: 6D grasping in cluttered scenes is a longstanding robotic manipulation problem. Open-loop manipulation pipelines can fail due to modularity and error sensitivity while most end-to-end grasping policies with raw perception inputs have not yet scaled to complex scenes with obstacles. In this work, we propose a new method to close the gap through sampling and selecting plans in the latent space. Our hierarchical framework learns collision-free target-driven grasping based on partial point cloud observations. Our method learns an embedding space to represent expert grasping plans and a variational autoencoder to sample diverse latent plans at inference time. Furthermore, we train a latent plan critic for plan selection and an option classifier for switching to an instance grasping policy through hierarchical reinforcement learning. We evaluate and analyze our method and compare against several baselines in simulation, and demonstrate that the latent planning can generalize to the real-world cluttered-scene grasping task.¹

Keywords: 6D Grasping in Cluttered Scenes, Robot Learning, Latent Planning

1 Introduction

6D robotic grasping of a specific object in cluttered scenes is important for common robotic applications such as a robot trying to pull out a cereal box from a shelf without moving other objects. Recently, there has been significant progress on using deep learning for grasp synthesis methods [1, 2, 3] and policy-based methods [4, 5, 6, 7] to tackle the grasping problem. However, the first approach has heavy reliance on the perception system and treats motion generation as a separate problem, while the second approach has not been shown to scale to challenging settings with obstacles. For complex and multi-modal robotics tasks [8, 9], we propose that end-to-end mapping from perception to low-level control can benefit from latent planning.

We consider target-driven grasping in clutter scenes [10] where collisions and unintended contact are more catastrophic than picking an object indiscriminately in a pile. In a standard motion and grasping planning pipeline [11, 12, 13], the model-based planners are often sensitive to estimated or approximated states such as object poses and shapes. Recent deep grasp synthesis methods [1, 2, 3] improves such limitations, but still execute motion plans in an open loop with information and metrics only before execution [14]. This modularity ignores the connection among perception and planning and control, and makes grasping challenging for cluttered scenes due to the heavy occlusions and potentials for collisions. On the other hand, most learning-based works concerning closed-loop grasping policy [4, 5, 6, 7] are restricted to output low-level actions such as joints or end effector poses from perception. They often lack the structures needed for complex scenarios that involve multi-modality and causality reasoning, and are limited to handle the bin picking scenarios or instance grasping without obstacles.

To fill in the gap between the cluttered-scene grasping paradigms, we propose to use representation learning and hierarchical policy to plan in the latent space [15, 16]. We posit that to improve an end-to-end policy on manipulation tasks that are challenging yet naturally have many solutions, we can exploit the multi-modality through considering the diverse plans rather than sticking to reach a single fixed goal. Therefore, we propose to represent the multi-modal grasping plans as latents and

¹Video and code can be found at <https://sites.google.com/view/latent-grasping>.

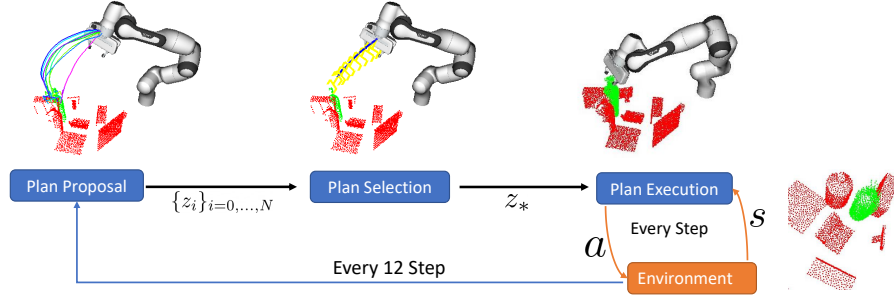


Figure 1: Illustration of the HCG framework. Our method learns a closed-loop hierarchical policy for cluttered scene grasping from segmented point clouds (green denotes target and red denotes obstacles). We learn a high-level latent plan sampler and a latent plan critic network to generate and select optimal plan. We then use a low-level plan-conditioned policy and a grasping primitive to avoid obstacles and execute grasping. The latent plans (colored lines) are visualized by recursively applying policy actions to the point clouds at current timestep in closed loop.

use latent plan sampling and selection mechanism to improve over the local nature of fixed-endpoint planning and low-level control.

Specifically, we adopt a workspace low-level control policy that takes partially-observed point clouds of objects as input. Given a latent vector that summarizes a nominal plan, the low-level policy is trained to avoid obstacles and approach the target. To compute a feasible latent plan, we train a generative model to sample latent plans through variational inference and a Q network to select latent plan through hierarchical reinforcement learning (HRL). Additionally, we jointly train a policy switch classifier to use a single-instance 6D grasping policy [6] for the final grasping stage. Our method reactively plans and controls for cluttered-scene grasping at test time, i.e. sample plans with high-level policy, choose a plan with high-level critic, execute the selected plan with low-level policy, and close the loop, shown in Fig. 1.

We conduct thorough analyses and evaluations on method components and choices in our hierarchical method for cluttered-scene 6D grasping. We demonstrate our latent sampler and critic can generate and select plan for this multi-modal task, and outperform several baselines in unseen test scenes in simulation. Finally, we evaluate the policy in the real world and show that the closed-loop end-to-end policy has robustness and generalization for obstacle avoidance and grasping success.

Overall, our contributions are: 1) We introduce an end-to-end cluttered-scene 6D grasping learning framework based on target-centric masked point clouds. 2) We propose Hierarchical policies for Cluttered-scene Grasping (HCG) to factorize a grasping plan as a latent vector that can be sampled from a generative model and can be executed with a plan-conditioned policy. We further improve the performance by learning a critic to select plan and a policy switch option [6] for the final grasping through online interactions. 3) We perform detailed experiments and validations in simulation and show that our policy can be successfully applied to challenging real-world cluttered scenes.

2 Related Work

Learning-based Cluttered-Scene Grasping: The vision-based cluttered-scene grasping literature largely concerns either 6D grasping synthesis for a single isolated object followed by postprocessing and planning [11, 12, 17, 2, 18, 10] or planar grasping policy for bin-picking scenarios [19, 4, 20]. Instead of learning top-down grasping policies to grasp rather small and light objects that are spread in a bin [7, 2], our method learns object-centric spatial grasping policy in clutters. Inspired by the recent works on state representations [6, 2, 10], our approach uses accumulated segmented scene point cloud as state to represent target and obstacles and reduces the sim-to-real perception gap.

Off-Policy Learning and Hierarchical Policy: We consider a model-free approach to tackle the sparse-reward grasping problem. Our work is related to policy methods that use demonstrations as priors to speed up learning and exploration [21, 22, 23] and hierarchical policies [24, 25, 26] that learn temporally extended actions or options. Decomposing long-horizon tasks into skill ab-

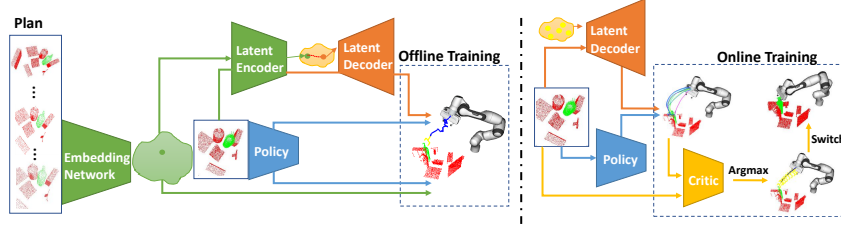


Figure 2: Illustration of our offline and online training procedure. Left) During offline stage, given a demonstration dataset, we jointly learn a plan embedding network, a plan sampler, and a low-level plan-conditioned policy. Right) During self-supervised online stage, we train a latent plan critic to select the optimal plan jointly with a GA-DDPG [6] option classifier to switch the low-level policy.

stractions or high-level actions are often shown to improve generalization and task transfer. Many works [27, 28, 29, 30] use subgoals or discrete actions as high-level action. For instance, [31] uses goal-conditioned low-level policy and high-level subgoal sampling and selection to learn sparse-reward tasks from demonstration data. Inspired by these methods, our work uses a motion and grasp expert planner [13] to provide demonstrations. Furthermore, our method uses high-level policy to generate abstract latent plans instead of goals for the low-level policy. Our work also uses a binary classifier to choose a pretrained grasping policy option [6] to improve success rates.

Behavior learning with Latent Variables: Latent variables have been used to represent complex skills in multi-task settings and to interpret the learned behavior semantics [15, 32, 33, 34, 16]. Since high-level behaviors are typically multi-modal, prior works have used generative models such as variational auto-encoder [35] and normalizing flow [36] to model the latent behavior distribution. For instance, [37] learns a transformed action space with RealNVP [38] and [16] uses cVAE to learn latent plans from plays for a plan-conditioned policy. These works often require goals as input at test time or only work with environments with limited scene variations and complexity such as contacts and obstacles. Instead, our work focuses on the multi-modality of potential grasping plans and uses latent variables in a conditional VAE to represent the diverse behaviors for obstacle avoidance and precision grasping in the context of cluttered-scene grasping. Moreover, We use HRL to train a critic network in order to select latent plans for a latent-conditioned closed-loop policy.

3 Learning Cluttered-Scene Grasping with Latent Plans

We use the standard notation of a Markov Decision Process (MDP): $\mathcal{M} = \{\mathcal{S}, \mathcal{R}, \mathcal{A}, \mathcal{P}, \rho_0, \gamma\}$. \mathcal{S} , \mathcal{A} , and \mathcal{O} represent the state, action, and observation space. $\mathcal{R} : \mathcal{S} \times \mathcal{A} \rightarrow \mathbb{R}$ is the reward function. $\mathcal{P} : \mathcal{S} \times \mathcal{A} \rightarrow \mathcal{S}$ is the transition dynamics. ρ_0 is the probability distribution over initial states and $\gamma = [0, 1)$ is a discount factor. To simplify the setting, we still use s to represent the input of the policy even though observations are used. Our goal is to learn a policy that maximizes the expected cumulative rewards $\mathbb{E}_\pi[\sum_{t=0}^{\infty} \gamma^t r_t]$, where r_t is the reward at time t . The Q-function of the policy for a state-action pair is $Q(s, a) = \mathcal{R}(s, a) + \gamma \mathbb{E}_{s', \pi}[\sum_{t=0}^{\infty} \gamma^t r_t | s_0 = s']$, where s' represents the next state of taking action a in state s according to the transition dynamics.

We consider the task of grasping a specific object from a cluttered scene without collisions, where observations come from a wrist camera mounted on the end-effector of a robot. Our objective is to learn a hierarchical grasping policy through offline and online training, shown in Fig. 2. The policy composes of a latent sampler $D_\phi : \mathcal{S} \times \mathbb{R} \rightarrow \mathcal{Z}$, a latent plan critic $Q : \mathcal{S} \times \mathcal{Z} \rightarrow \mathbb{R}$, and a low-level policy $\pi : \mathcal{S} \times \mathcal{Z} \rightarrow \mathcal{A}$ where \mathcal{Z} represents the plan embedding space. At each planning timestep t , an embedding vector z_t is sampled by D_ϕ and selected by Q to represent a plan. At each environment step, the low-level policy π takes the observation s_t and the latent plan z_t to output action a_t as the relative 3D translation and the 3D rotation of the robot end-effector.

3.1 Latent Plan Embedding and Plan-Conditioned Policy

We use accumulated 3D segmented point cloud representation [6] in the egocentric view to represent the state s_t . The point cloud is augmented with a binary mask to specify the target, the current joint angles to consider arm collision, and the remaining timestep to provide horizon information.

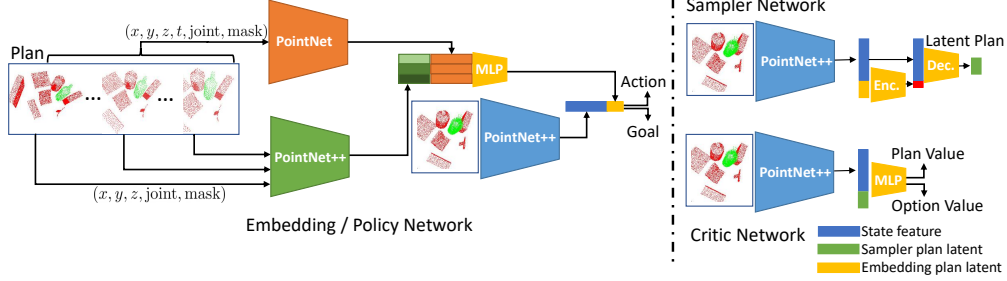


Figure 3: Illustration of the network architectures. Left) Network architecture for the embedding network and low-level policy. Right) Network architecture for the VAE sampler and critic network.

To train a policy on a cluttered-scene grasping dataset with potentially many modes (e.g. different ways to grasp a bowl), we can condition the policy on the plan [16] such that the low-level policy only needs to learn uni-modal behavior. We adopt OMG planner [13] as the expert due to its flexibility in choosing grasping goals in cluttered scenes. We model the plan as a sequence of point clouds through transforming the current observation s_t by relative poses in the plan. Note that the point cloud at each time step shares the same canonical geometry with poses factored out, so the network needs to encode the trajectory path with the scene geometry. We consider a plan to be different from an actual rollout since the plan is abstracted from noises and dynamics and needs to be inferred from the current state. Specifically, the rollout τ is generated by executing a perturbed version of the expert plan to mitigate the distribution shift for standard behavior cloning [39, 40] and it has information that is not present in the current state s_t due to partial views. We leave some details and discussions to Appendix 6.1.2.

In Fig. 3, we use a spatiotemporal architecture [41] denoted as θ to encode the 4D point cloud trajectory as a global plan embedding vector z_θ , which is then concatenated with the current observation for the low-level policy π to generate actions. Let a and g be the action and goal predicted from the policy $\pi(s, z_\theta)$, and a^* be the expert action and g^* be the goal in the plan. We minimize the behavior cloning loss and the goal auxiliary loss [6] jointly to align the intent of the learner behavior to the expert. For a single trajectory, the embedding network and the low level policy are trained with the supervised learning loss

$$L_{\text{traj}}(z_\theta, \pi) = \frac{1}{T} \sum_i^T (L_{\text{POSE}}(g_i, g_i^*) + L_{\text{POSE}}(a_i, a_i^*)) \quad (1)$$

where L_{POSE} [6] is the point matching loss for a set of predefined gripper points to optimize translation and rotation.

3.2 Latent Plan Proposal with A Generative Model

With the access to a single expert demonstration or plan at test time, the plan embedding network can encode the plan such that the low-level policy can follow it to avoid obstacles and execute grasping. However, since we want to lift this assumption and generalize to unseen scenes, we propose to use a variational inference framework[35] to generate latent plans. The objective of the latent plan sampler is to model the distribution of state observation and expert embedding to provide multi-modal plans at inference time. Instead of jointly modeling plan embedding and sampler distributions [16], we learn latents for plan embedding, similar to hierarchical variational autoencoders. Conditional variational autoencoder (cVAE), denoted as ϕ , uses parametrized encoder E_ϕ and decoder D_ϕ to maximize the marginal log likelihood of observations $\log_\phi(z_\theta|s)$, i.e. to generate the expert plan embedding conditioned on current observations. The Evidence Lower Bound (ELBO) for cVAE can be written as

$$\log p_\phi(z|s) \geq -\text{KL}(q(c|z, s)||p(c)) + \mathbb{E}_{q(c|z, s)}[\log p(z|c, s)] \quad (2)$$

where $c = E_\phi(s, z)$ denotes the latent from encoding plan z conditioned on state s and the prior distribution $p(c)$ is restricted to be a 2-dimension unit gaussian. In Fig. 4, we compare the learned 2D latent space \mathcal{C} to a 2-dimensional t-SNE[42] on the embedding space \mathcal{Z} .

We maximize ELBO with a regularization loss $L_{\text{KL}} = \text{KL}(\mathcal{N}(\mu_\phi, \text{diag}(\sigma_\phi^2))||\mathcal{N}(\mathbf{0}, I_2))$ and a latent reconstruction loss $L_{\text{recons}} = \|z_\theta - z_\phi\|_2^2$ where we parametrize the encoder with mean μ_ϕ and

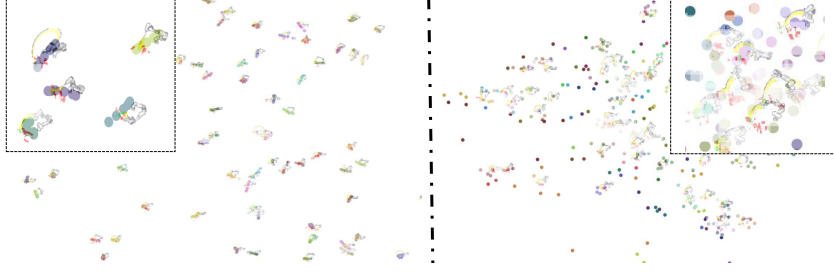


Figure 4: Comparison of t-SNE embeddings and VAE embeddings of latent plans z_θ where states in the same trajectory are denoted by the same color. Left) The 2-dimension t-SNE embedding of \mathcal{Z} shows that our embedding network θ implicitly learns to distinguish plan embeddings from different trajectories and cluster embeddings for states in the same trajectory. Right) The 2-dimension VAE latent \mathcal{C} shows that VAE learning objective balances between representing salient plan features and regularizing with the gaussian prior.

diagonal covariance σ_ϕ and use reparametrization tricks to sample z_ϕ . Additionally, the sampler latent z_ϕ can be further decoded with the low-level policy $\pi(s, z_\phi)$ on the expert trajectory to minimize the plan loss in Eq. 1. In this way, the action and goal losses from $L_{\text{traj}}(z_\phi, \pi)$ can also provide gradient information such that the latent generated by ϕ acts similar to the expert plan latent z_θ . Therefore, the total loss is

$$L_{\text{sampler}} = \beta L_{\text{KL}} + L_{\text{recons}} + L_{\text{traj}}(z_\phi, \pi) \quad (3)$$

where β is a hyperparameter [43]. Algorithm 1 summarizes the joint training of plan embedding and sampler network. At test time, we can use $D_\phi(s, c)$ to decode samples $c \sim \mathcal{C}$ to for executable plan embeddings. For multi-modal tasks and data, reasoning in the plan space through generative models improves local behaviors such as obstacle avoidance.

3.3 Hierarchical RL for Latent Plan Critic and Policy Switch

A hierarchical framework is desirable for efficient continual online learning on unknown objects and scenes. Because the low-level policy can help avoid the risks and expenses of random explorations while the high-level policy can focus on adapting policy learning for the abstract actions. In our method, the high-level action contains a continuous latent plan z_ϕ sampled from D_ϕ and a binary policy option to switch from the low-level policy from π to a pretrained GA-DDPG policy [6]. The selected low-level closed-loop policy then executes the workspace control a . The goal is to learn plan and policy selection through online experience in collision avoidance and grasping affordance.

We use Q learning [44] to train the plan critic $Q(s_t, z)$ to predict the value of starting from current state s_t and following the plan z . Compared with learning on low-level actions $Q(s_t, a_t)$ where the critic needs to implicitly reason over the credit assignment, the trajectory latent vector z provides information on the entire trajectory. Moreover, we can learn an option classifier $G(s_t)$ to choose the binary policy option. $G(s_t)$ learns to predict the episode success if we start using GA-DDPG as a single-object grasping primitive from the current state s_t and a high $G(s_t)$ means that we can switch the low-level policy at s_t . We jointly learn the critic $Q(s_t, z)$ and the GA-DDPG option classifier $G(s_t)$ by augmenting GA-DDPG execution from a random timestep t_{switch} at the end of each rollout. The final episode reward can be used as labels for $G(s_t)$ in timesteps after t_{switch} since future policy switch would not change the reward.

We use sparse rewards for the MDP: An episode terminates once a grasp succeeds with reward 1, a collision happens with reward -1, or 0 in other cases. We use a mixture of return and bootstrapped next-state value as the target for Bellman equation $y_t = \lambda(r(s_t, z_t) + \gamma \max_{z' \sim \phi(s_{t+1})} Q(s_{t+1}, z')) + (1 - \lambda)\gamma^T r_T$ where $\lambda = 0.5$. We also denote the episode success indicator $r_T^\pm = 1$ if $r_T = 1$ and 0 otherwise. The final loss for the critic is

$$L_{\text{critic}} = (Q(s_t, z_t) - y_t)^2 + \text{BCE}(G(s_t), r_T^\pm) \cdot \mathbb{1}(t \geq t_{\text{switch}}) \quad (4)$$

where the first term is Bellman error and BCE denotes the binary cross entropy loss. The on-policy training algorithm for critic and option classifier is summarized in Algorithm 2. At test time

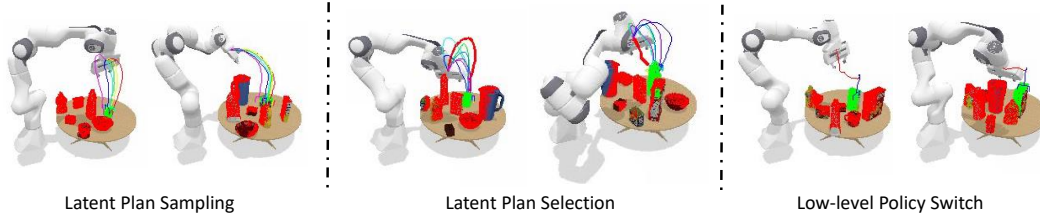


Figure 5: Qualitative analysis of the method components. Left) We observe some diverse plans generated from the plan sampler network. We smoothly modify one latent coordinate and observe the corresponding plan transitions, colored from red to magenta in the HSV space. Middle) The latent plan critic selects the maximum value trajectory (colored in red) among samples. Right) The policy transition from a plan trajectory (red) to a target-specific grasping trajectory (blue).

Test	BC	GA-DDPG	BC Residual	WayPoint	Rollout Encoding	Plan Encoding
Reward	0.128 \pm 0.03	-0.240 \pm 0.05	0.273 \pm 0.02	0.044 \pm 0.02	0.463 \pm 0.04	0.600 \pm 0.03
Success	0.437 \pm 0.02	0.328 \pm 0.02	0.463 \pm 0.01	0.356 \pm 0.03	0.618 \pm 0.03	0.705 \pm 0.02
Collision	0.308 \pm 0.03	0.570 \pm 0.03	0.190 \pm 0.02	0.312 \pm 0.02	0.157 \pm 0.01	0.104 \pm 0.01

Table 1: Rewards, success, and collisions of different policy methods. Mean and one standard deviation are provided.

for every 12 environment steps, we will resample 8 trajectory candidates for the critic to select an optimal plan and filter out the suboptimal ones. We will switch to GA-DDPG if $G(s_t) > 0.5$ and this improves the success from our experiments since GA-DDPG is specifically targeted to grasp single object from proximity compared to a general behavior-conditioned low-level policy. Examples of plan sampling, selection and policy switch are shown in Fig. 5.

4 Experiments

We conduct experiments and present our findings to the following questions. (1) Given an expert plan, how well do trajectory encoding network and plan-conditioned policy behave compared with other end-to-end baselines? (2) Does the cVAE generative model learn diverse and feasible planning behavior for unseen test scenes? (3) Can the latent critic and GA-DDPG policy classifier trained with HRL further improve the performance? We also conduct ablation studies on different components, a comparison with open-loop baselines, and real-world experiments for cluttered-scene 6D grasping.

Simulation Task Environment. We experiment with the Franka Emika Panda arm, a 7-DOF arm with a parallel gripper. We use ShapeNet [45] and YCB objects [46] as the object repository and the Acronym [47] grasp set for OMG planner. A task scene is generated by first placing a target object, and then setting up to 8 obstacles with random stable poses on a table in the PyBullet Simulator [48]. The maximum horizon for the policy is $T = 50$. The MDP is sparse-reward: An episode succeeds with reward 1, collides with reward -1 , or 0 in other cases.

Training and Testing. We use approximately 1,500 ShapeNet objects from 169 different classes for offline training and YCB scenes for online interactions. For testing, we use 9 selected YCB objects with 20 unseen scenes per object. We run each scene 5 times and compute the statistics of grasping success rates, collision rates, and rewards. More details can be found in Appendix 6.1.

4.1 Plan Embedding and Trajectory Execution

We conduct experiments to investigate the performance of the embedding representation and the low-level policy. In Table 1, we can see that i) Vanilla end-to-end behavior clone does not perform very well, possibly due to the multi-modal trajectory demonstrations. The state space for grasping in clutters is also more complex than single object grasping. ii) Directly running pretrained GA-DDPG policy without considering the obstacles has heavy collisions. A standard extension is to learn a residual policy [49] in addition to GA-DDPG, which also performs suboptimally. iii) A vanilla planning network that outputs trajectory waypoints behaves similar to BC because the extended action does not solve the problem. The closed-loop observation-conditioned controller are more suitable for executing the long-horizon rollout. iv) The model that encodes noisy and dynamics-involved rollout performs worse than plan encoding. Overall, the path geometry and lo-

Test	Regress	Vanilla VAE	Zeros	No Policy Loss	Single Plan	Plan VAE
Reward	0.369 +- 0.01	-0.460 +- 0.02	0.385 +- 0.04	0.400 +- 0.05	0.492 +- 0.02	0.536 +- 0.03
Success	0.600 +- 0.01	0.022 +- 0.01	0.543 +- 0.02	0.528 +- 0.05	0.601 +- 0.02	0.637 +- 0.02
Collision	0.231 +- 0.01	0.483 +- 0.02	0.158 +- 0.01	0.126 +- 0.01	0.110 +- 0.01	0.101 +- 0.01

Table 2: Mean and standard deviations of rewards, success, and collisions of different models that are used to generate the trajectory latent.

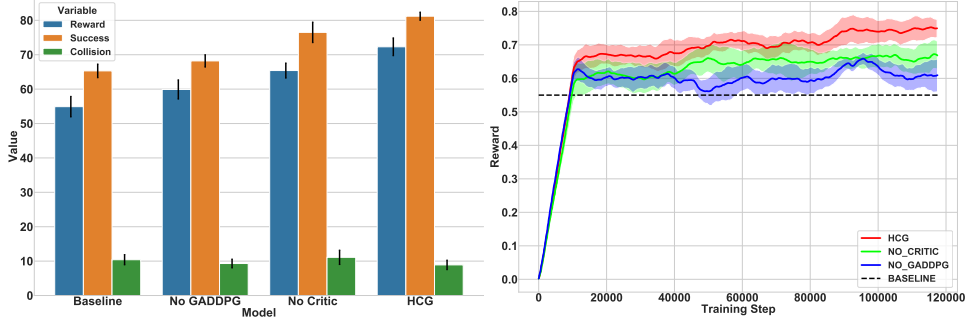


Figure 6: Left) Ablation study on the self-supervision stage. Right) The mean and the 1 standard deviation for the reward plots. We observe that a combination of plan selection and GA-DDPG option improves the performance.

cal observation information in the latent plan enables the plan-conditioned policy to perform better than naive end-to-end baselines. Furthermore, we observe that the low-level policy learns reactive behaviors to avoid obstacles in addition to trajectory following.

4.2 Generative Models for Latent Plans

We evaluate the model performance of different latent planners based on the same low-level policy and embedding network. In Table 2, we can see that i) Latent regression models can have troubles providing useful plan information for novel test scenes. A cVAE models the joint state and latent distribution and better captures the multi-modality in the plan space. We also observe that models trained without a separate latent VAE network [16, 34] tend to collapse the plans during inference. ii) A vanilla 64 dimension latent VAE (trained with no hierarchy on z) only provides a unit gaussian sample to the low-level policy and is not sufficient to represent useful behaviors. iii) A dummy zero latent also does not provide as much information to the low-level policy. iv) Compared to only reconstruct latents, the policy loss improves the latent model. v) Reactive sampling new plans in a closed loop is better than adopting a single plan for the entire execution. Finally, although we lift the expert plan requirement, inferring latent plans still outperforms simple end-to-end policies.

Since the low-level policy is trained to map from the current observation and latent to goals and actions, meaningful latent covers plans both to curve around obstacles and to reach diverse goals. When the latent is not meaningful, the policy often struggles with local behaviors such as using a straight plan to reach the nearest goal. Compared with goal generation and goal-conditioned policy [28, 29, 16] that requires image goal as input, our model does not make such assumption and aims to generalize to various scenes and objects with different geometry.

4.3 Hierarchical Reinforcement Learning

Our policy trained on offline demonstration data and ShapetNet objects achieves reward around 0.54 in average as shown in Table 2. Compared to pure learning from demonstrations, the hierarchical RL procedure trains the critic and the GA-DDPG option classifier on new scenes with interactions. Shown in Fig. 6, we observe an improvement in the final reward for the policy and plan selection components. The trials and errors enforce the critic to learn a useful scoring function that improves stability and collision in hard scene instances. On test scenes, our final hierarchical policy can reach a mean performance of 81.2% success with only 8.9% collision.

The latent plan score summarizes both the obstacle vicinity and the grasp quality. When avoiding large obstacles, we observe the critic’s preference over plans that are far from obstacles. As plans correspond to diverse grasps in clear spaces, the scores are used to rank grasp feasibility. Moreover,

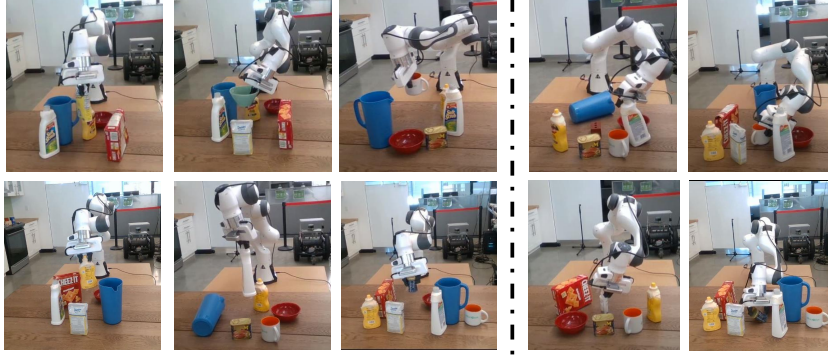


Figure 7: Successes (left) and failures (right) of real-world tabletop cluttered-scene grasping using our policy trained in simulation. The target object is surrounded by obstacles and the robot initial configuration is varying for each scene.

GA-DDPG is crucial to align the grasping pose to improve the final grasping success rates. Note that the sampled latent can be rolled out with only current observation by transforming the point cloud. When abstract plans are hard to distinguish or reason over, the plan can be further combined with analytic trajectory scoring methods or trajectory optimizers before execution. Some additional discussions on the limitations and potential improvements can be found in Appendix 6.2.

4.4 Comparison with Open-Loop Baselines

We compare our method against a state-of-the-art grasp detection method 6DGraspNet [3, 10] and a cluttered-scene method Contact-Graspnet [50] in simulation. The manipulation pipeline approximates the scene SDF with point clouds and runs grasp detection methods to generate diverse grasps as goal sets for planning [13]. The open-loop method with 6DGraspNet achieves 67.2% success rate with 19.0% collisions and the one with Contact-Graspnet achieves 72.2% success rate with 16.4% collision rates due to better grasps. Note that the simulation test scenes have a variety of occlusions and obstacles, which makes the motion and grasp planning pipeline difficult. Overall, the improvements in our method shows the flexibility of a closed-loop hierarchical policy.

4.5 Tabletop Cluttered-Scene Grasping in the Real World

We conduct real-world grasping experiments with HCG. To obtain the segmented point cloud of an object in tabletop settings, we utilized an unseen object instance segmentation method [51]. The latent plan sampling and selection takes around 0.2s and the low-level policy runs in around 25 Hz. Fig. 7 shows some qualitative results in our experiments. The target object is surrounded by obstacles which causes heavy occlusions and challenges in collision avoidance. The robot uses the same testing procedure as in simulation and grasped each target object 5 times with varying robot initial configurations. The policy trained only in simulation generalizes well to the real world and we observe feasible plans to avoid arm collisions and smooth low-level controls that grasp objects in challenging cluttered scenes. The overall policy succeeds with 21 trials out of 34 attempts on 8 challenging test scenes. The majority of grasping failures are due to slippery contacts caused by sim-to-real physics gap and slight collisions after switching to GA-DDPG.

5 Conclusion

We introduce Hierarchical policies for Cluttered-scene Grasping (HCG), an end-to-end method to grasp in clutters from point clouds. The task is common in unstructured human environments and yet is challenging for current policy methods for its complexity in partial views and collision avoidance. Our method learns a latent plan sampler through variational autoencoder and a latent plan critic through Q learning. Our hierarchical policy also uses a single-instance grasping policy as an action primitive to improve the grasping accuracy. The overall system achieves robustness and generalization across diverse unseen scenes and robot initial configurations both in simulation and the real world. A key limitation of our trained policy in the real world is the sim-to-real gap in contacts during grasping, where real-world finetuning with reinforcement learning can be helpful.

References

- [1] J. Redmon and A. Angelova. Real-time grasp detection using convolutional neural networks. In *IEEE International Conference on Robotics and Automation (ICRA)*, pages 1316–1322, 2015.
- [2] J. Mahler, J. Liang, S. Niyaz, M. Laskey, R. Doan, X. Liu, J. A. Ojea, and K. Goldberg. Dex-net 2.0: Deep learning to plan robust grasps with synthetic point clouds and analytic grasp metrics. *Robotics: Science and Systems (RSS)*, 2017.
- [3] A. Mousavian, C. Eppner, and D. Fox. 6-DOF GraspNet: Variational grasp generation for object manipulation. In *International Conference on Computer Vision (ICCV)*, pages 2901–2910, 2019.
- [4] D. Kalashnikov, A. Irpan, P. Pastor, J. Ibarz, A. Herzog, E. Jang, D. Quillen, E. Holly, M. Kalakrishnan, V. Vanhoucke, and S. Levine. Qt-opt: Scalable deep reinforcement learning for vision-based robotic manipulation. *arXiv preprint arXiv:1806.10293*, 2018.
- [5] D. Quillen, E. Jang, O. Nachum, C. Finn, J. Ibarz, and S. Levine. Deep reinforcement learning for vision-based robotic grasping: A simulated comparative evaluation of off-policy methods. In *IEEE International Conference on Robotics and Automation (ICRA)*, pages 6284–6291, 2018.
- [6] L. Wang, Y. Xiang, and D. Fox. Goal-auxiliary actor-critic for 6d robotic grasping with point clouds. *arXiv preprint arXiv:2010.00824*, 2020.
- [7] S. Song, A. Zeng, J. Lee, and T. Funkhouser. Grasping in the wild: Learning 6DoF closed-loop grasping from low-cost demonstrations. *Robotics and Automation Letters*, 2020.
- [8] A. Sadat, S. Casas, M. Ren, X. Wu, P. Dhawan, and R. Urtasun. Perceive, predict, and plan: Safe motion planning through interpretable semantic representations. In *European Conference on Computer Vision*, pages 414–430. Springer, 2020.
- [9] Y. C. Nakamura, D. M. Troniak, A. Rodriguez, M. T. Mason, and N. S. Pollard. The complexities of grasping in the wild. In *2017 IEEE-RAS 17th International Conference on Humanoid Robotics (Humanoids)*, pages 233–240. IEEE, 2017.
- [10] A. Murali, A. Mousavian, C. Eppner, C. Paxton, and D. Fox. 6-DOF grasping for target-driven object manipulation in clutter. In *IEEE International Conference on Robotics and Automation (ICRA)*, 2020.
- [11] N. Kitaev, I. Mordatch, S. Patil, and P. Abbeel. Physics-based trajectory optimization for grasping in cluttered environments. In *2015 IEEE International Conference on Robotics and Automation (ICRA)*, pages 3102–3109. IEEE, 2015.
- [12] M. Dogar and S. Srinivasa. A framework for push-grasping in clutter. *Robotics: Science and systems VII*, 1, 2011.
- [13] L. Wang, Y. Xiang, and D. Fox. Manipulation trajectory optimization with online grasp synthesis and selection. In *Robotics: Science and Systems (RSS)*, 2020.
- [14] D. Kappler, F. Meier, J. Issac, J. Mainprice, C. G. Cifuentes, M. Wüthrich, V. Berenz, S. Schaal, N. Ratliff, and J. Bohg. Real-time perception meets reactive motion generation. *IEEE Robotics and Automation Letters*, 3(3):1864–1871, 2018.
- [15] K. Hausman, J. T. Springenberg, Z. Wang, N. Heess, and M. Riedmiller. Learning an embedding space for transferable robot skills. In *International Conference on Learning Representations*, 2018.
- [16] C. Lynch, M. Khansari, T. Xiao, V. Kumar, J. Thompson, S. Levine, and P. Sermanet. Learning latent plans from play. In *Conference on Robot Learning*, pages 1113–1132. PMLR, 2020.
- [17] L. Pinto and A. Gupta. Supersizing self-supervision: Learning to grasp from 50k tries and 700 robot hours. In *IEEE International Conference on Robotics and Automation (ICRA)*, pages 3406–3413, 2016.

- [18] D. Morrison, P. Corke, and J. Leitner. Closing the loop for robotic grasping: A real-time, generative grasp synthesis approach. In *Robotics: Science and Systems (RSS)*, 2018.
- [19] S. Levine, P. Pastor, A. Krizhevsky, J. Ibarz, and D. Quillen. Learning hand-eye coordination for robotic grasping with deep learning and large-scale data collection. *The International Journal of Robotics Research (IJRR)*, 37(4-5):421–436, 2018.
- [20] S. Iqbal, J. Tremblay, A. Campbell, K. Leung, T. To, J. Cheng, E. Leitch, D. McKay, and S. Birchfield. Toward sim-to-real directional semantic grasping. In *IEEE International Conference on Robotics and Automation (ICRA)*, pages 7247–7253, 2020.
- [21] A. Rajeswaran, V. Kumar, A. Gupta, G. Vezzani, J. Schulman, E. Todorov, and S. Levine. Learning complex dexterous manipulation with deep reinforcement learning and demonstrations. *arXiv preprint arXiv:1709.10087*, 2017.
- [22] M. Vecerik, T. Hester, J. Scholz, F. Wang, O. Pietquin, B. Piot, N. Heess, T. Rothörl, T. Lampe, and M. Riedmiller. Leveraging demonstrations for deep reinforcement learning on robotics problems with sparse rewards. *arXiv preprint arXiv:1707.08817*, 2017.
- [23] A. Nair, B. McGrew, M. Andrychowicz, W. Zaremba, and P. Abbeel. Overcoming exploration in reinforcement learning with demonstrations. In *IEEE International Conference on Robotics and Automation (ICRA)*, pages 6292–6299, 2018.
- [24] M. Stolle and D. Precup. Learning options in reinforcement learning. In *International Symposium on abstraction, reformulation, and approximation*, pages 212–223. Springer, 2002.
- [25] R. S. Sutton, D. Precup, and S. Singh. Between mdps and semi-mdps: A framework for temporal abstraction in reinforcement learning. *Artificial intelligence*, 112(1-2):181–211, 1999.
- [26] P.-L. Bacon, J. Harb, and D. Precup. The option-critic architecture. In *Proceedings of the AAAI Conference on Artificial Intelligence*, volume 31, 2017.
- [27] O. Nachum, S. Gu, H. Lee, and S. Levine. Data-efficient hierarchical reinforcement learning. *arXiv preprint arXiv:1805.08296*, 2018.
- [28] A. Nair, V. Pong, M. Dalal, S. Bahl, S. Lin, and S. Levine. Visual reinforcement learning with imagined goals. In *Advances in Neural Information Processing Systems (NeurIPS)*, pages 9191–9200, 2018.
- [29] C. Florensa, D. Held, X. Geng, and P. Abbeel. Automatic goal generation for reinforcement learning agents. In *International Conference on Machine Learning (ICML)*, pages 1515–1528, 2018.
- [30] A. Simeonov, Y. Du, B. Kim, F. R. Hogan, J. Tenenbaum, P. Agrawal, and A. Rodriguez. A long horizon planning framework for manipulating rigid pointcloud objects. *arXiv preprint arXiv:2011.08177*, 2020.
- [31] A. Mandlekar, F. Ramos, B. Boots, S. Savarese, L. Fei-Fei, A. Garg, and D. Fox. Iris: Implicit reinforcement without interaction at scale for learning control from offline robot manipulation data. In *2020 IEEE International Conference on Robotics and Automation (ICRA)*, pages 4414–4420. IEEE, 2020.
- [32] B. Eysenbach, A. Gupta, J. Ibarz, and S. Levine. Diversity is all you need: Learning skills without a reward function. *arXiv preprint arXiv:1802.06070*, 2018.
- [33] Y. Li, J. Song, and S. Ermon. Infogail: Interpretable imitation learning from visual demonstrations. *arXiv preprint arXiv:1703.08840*, 2017.
- [34] K. Pertsch, Y. Lee, and J. J. Lim. Accelerating reinforcement learning with learned skill priors. *arXiv preprint arXiv:2010.11944*, 2020.
- [35] D. P. Kingma and M. Welling. Auto-encoding variational bayes. *arXiv preprint arXiv:1312.6114*, 2013.

- [36] D. Rezende and S. Mohamed. Variational inference with normalizing flows. In *International Conference on Machine Learning*, pages 1530–1538. PMLR, 2015.
- [37] A. Singh, H. Liu, G. Zhou, A. Yu, N. Rhinehart, and S. Levine. Parrot: Data-driven behavioral priors for reinforcement learning. *arXiv preprint arXiv:2011.10024*, 2020.
- [38] L. Dinh, J. Sohl-Dickstein, and S. Bengio. Density estimation using real nvp. *arXiv preprint arXiv:1605.08803*, 2016.
- [39] S. Ross, G. Gordon, and D. Bagnell. A reduction of imitation learning and structured prediction to no-regret online learning. In *International Conference on Artificial Intelligence and Statistics (AISTATS)*, pages 627–635, 2011.
- [40] M. Laskey, J. Lee, R. Fox, A. Dragan, and K. Goldberg. Dart: Noise injection for robust imitation learning. In *Conference on robot learning*, pages 143–156. PMLR, 2017.
- [41] D. Rempe, T. Birdal, Y. Zhao, Z. Gojcic, S. Sridhar, and L. J. Guibas. Caspr: Learning canonical spatiotemporal point cloud representations. In *Advances in Neural Information Processing Systems (NeurIPS)*, 2020.
- [42] L. Van der Maaten and G. Hinton. Visualizing data using t-sne. *Journal of machine learning research*, 9(11), 2008.
- [43] I. Higgins, L. Matthey, A. Pal, C. Burgess, X. Glorot, M. Botvinick, S. Mohamed, and A. Lerchner. beta-vae: Learning basic visual concepts with a constrained variational framework. 2016.
- [44] H. Van Hasselt, A. Guez, and D. Silver. Deep reinforcement learning with double q-learning. In *Thirtieth AAAI conference on artificial intelligence*, 2016.
- [45] A. X. Chang, T. Funkhouser, L. Guibas, P. Hanrahan, Q. Huang, Z. Li, S. Savarese, M. Savva, S. Song, H. Su, et al. Shapenet: An information-rich 3d model repository. *arXiv preprint arXiv:1512.03012*, 2015.
- [46] B. Calli, A. Walsman, A. Singh, S. Srinivasa, P. Abbeel, and A. Dollar. Benchmarking in manipulation research: The YCB object and model set and benchmarking protocols. *IEEE Robotics and Automation Magazine*, 22(3):36–52, 2015.
- [47] C. Eppner, A. Mousavian, and D. Fox. ACRONYM: A large-scale grasp dataset based on simulation. In *2021 IEEE Int. Conf. on Robotics and Automation, ICRA*, 2020.
- [48] E. Coumans and Y. Bai. PyBullet, a python module for physics simulation for games, robotics and machine learning. <http://pybullet.org>, 2016–2019.
- [49] T. Silver, K. Allen, J. Tenenbaum, and L. Kaelbling. Residual policy learning. *arXiv preprint arXiv:1812.06298*, 2018.
- [50] M. Sundermeyer, A. Mousavian, R. Triebel, and D. Fox. Contact-graspnet: Efficient 6-dof grasp generation in cluttered scenes. *arXiv preprint arXiv:2103.14127*, 2021.
- [51] Y. Xiang, C. Xie, A. Mousavian, and D. Fox. Learning RGB-D feature embeddings for unseen object instance segmentation. In *Conference on Robot Learning (CoRL)*, 2020.
- [52] C. R. Qi, L. Yi, H. Su, and L. J. Guibas. PointNet++: Deep hierarchical feature learning on point sets in a metric space. In *Advances in Neural Information Processing Systems (NeurIPS)*, pages 5099–5108, 2017.
- [53] C. R. Qi, H. Su, K. Mo, and L. J. Guibas. Pointnet: Deep learning on point sets for 3d classification and segmentation. In *Proceedings of the IEEE conference on computer vision and pattern recognition*, pages 652–660, 2017.
- [54] D. P. Kingma and J. Ba. Adam: A method for stochastic optimization. *arXiv preprint arXiv:1412.6980*, 2014.
- [55] S. Fujimoto, H. Van Hoof, and D. Meger. Addressing function approximation error in actor-critic methods. *arXiv preprint arXiv:1802.09477*, 2018.

6 Appendix

Algorithm 1: Plan Embedding and Sampler Training (demonstration D_{offline})

```

for  $i = 0, \dots, N$  do
  Initialize low-level policy  $\pi$ , plan embedding network  $\theta$ , plan sampler  $\phi$ 
  Sample a rollout  $\tau_t = \{(s_t, a_t, g_t), \dots, (s_T, a_T, g_T)\}$  and plan  $\xi_t$  from  $D_{\text{offline}}$ 
  Encode  $\xi_t$  into  $z_\theta$  and optimize  $\pi, \theta$  on  $\tau_t$  with Eq. (1)
  Autoencode  $z_\theta$  into  $z_\phi$  and optimize  $\phi$  on  $\tau_t$  with Eq. (3)
end

```

Algorithm 2: Critic Training (plan sampler ϕ , low-level policy π)

```

for  $i = 0, \dots, N$  do
  Initialize critic  $Q$ , policy option classifier  $G$ , dataset  $D_{\text{online}}$ , and switch step  $t_{\text{switch}}$ 
  Execute  $\pi$  with sampled latent  $z$  for  $t_{\text{switch}}$  steps and switch to GA-DDPG policy
  Log trajectory  $\tau = (s_0, a_0, r_0, z_0, \dots, s_T, a_T, r_T, z_T)$  to  $D_{\text{online}}$ 
  Sample a transition  $(s_t, z_t, r_t, s_{t+1})$  with episode information  $r_T, t_{\text{switch}}$  from  $D_{\text{online}}$ 
  Optimize  $Q, G$  with Eq. (4)
end

```

6.1 Implementation Details

6.1.1 Task and Environment Details

Each observation in PyBullet has RGB, depth, and mask images with height and width 224. We backproject the scene point clouds from the foreground masks. Following [6], we use accumulated segmented point cloud representations in the egocentric view to represent the state s_t . The point cloud state is augmented with a mask channel to specify the target, i.e. 0 represents target and 1 represents obstacles. To provide the agent with enough information to avoid arm collisions, we concatenate the current joint angles to the point clouds as extra 9 dimensions. We choose the robot base coordinate frame to aggregate the 3D points. Each timestep we will add new observed points to the global aggregated points and use farthest point sampling [52] as a downsampling scheme to limit the number of total points. The final network input contains 4096 sampled points from the state s_t where 1024 points for the target and the rest for obstacles. The point aggregation is important for ego-view agents in cluttered scene grasping whenever possible since previous observations provide important information and the wrist camera can lose views during collision avoidance.

For the action parametrization, we adopt workspace control for its alignments with the observation space and learning performance. We randomize the initial states ρ_0 from a uniform pose distribution above the table facing toward the target object, in a distance from 0.6 meter to 0.8 meter. we use the depth region between the two fingertips to determine if the robot should close the fingers and retract the arm to complete a grasp. We have experimented with adding sampled robot arm point clouds and table point clouds, as well as computing nearest collision point distances and object point normals as inputs, and did not observe performance improvements. Instead of modeling collision-specific features or designing analytic cost functions, the high-level latent critic learns collision-avoidance from the sparse collision rewards through interactions.

6.1.2 Plan Details

Let $\xi_t = (\mathcal{T}_t, \mathcal{T}_{t+1}, \dots, \mathcal{T}_T)$ be a trajectory of the robot gripper pose generated from the OMG planner to grasp an object at state s_t , where $\mathcal{T}_t \in \mathbb{SE}(3)$ is the gripper pose in the robot base frame at time t . Then the expert action at time t can be computed as $a_t^* = \mathcal{T}_{t+1}\mathcal{T}_t^{-1}$, which is the relative transformation of the gripper between t and $t+1$. Furthermore, \mathcal{T}_T from the planner is a successful grasp pose of the object. We define the expert goal at time t as $g_t^* = \mathcal{T}_T\mathcal{T}_t^{-1}$, which is the relative transformation between the current gripper pose and the final grasp. Given the point cloud s_t at the current state and the plan ξ_t , we can represent the plan observations as a sequence of point clouds

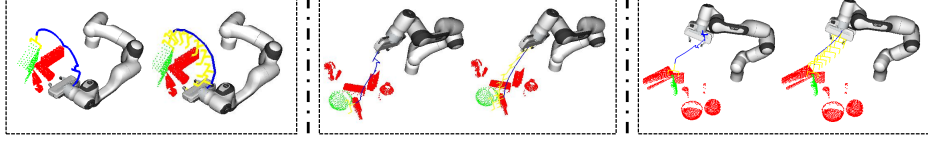


Figure 8: Examples of comparisons between the noisy rollouts (left) and expert plan (right). The trajectories are denoted with blue lines, and goals and sampled states are denoted as yellow grippers.

from $t + 1$ to T based on the poses in the plan, i.e. $\hat{s}_{t+i} = \mathcal{T}_{t+i}\mathcal{T}_t^{-1}(s_t)$. We also concatenate the normalized trajectory time $\{0, 1/(T - t), \dots, 1\}$ and joints q_t, \dots, q_T to each of the point cloud in the plan. To fit into the GPU memory, the point cloud trajectory $\{s_t, \hat{s}_{t+1}, \dots, \hat{s}_T\}$ is evenly downsampled with ratio 6 and the supervised trajectory states are randomly downsampled with ratio 5. We include both end points for trajectory encoding and supervision, so the final trajectory length is in between 2 and 11 for a horizon of 50. A rollout can be distinct from a plan since we add perturbation noises [40] to the expert trajectory, as shown in Fig. 8. The planner would efficiently re-plan to the same goal with the remaining horizon when we perturb the trajectory. We emphasize the difference between plan and rollout is not to demand a planner as a strict requirement. For instance, a real-world trajectory rollout dataset can be expensive to acquire and contain environment noises, yet diverse high-level sketch plans can be clean and still easy to provide. This is used to improve training performance for the low-level policy and the latent plan space in our experiments.

6.1.3 Network Details

Shown in Fig. 3, our plan embedding network is similar to [41]. The PointNet++ [52] is used to capture the local geometry while the PointNet [53] is used to capture the global plan information. We use three point set abstraction layers for PointNet++. The variable-length trajectory features for each point clouds are then max-pool into a global feature z_θ of dimension 64. For the trajectory latent autoencoder, we use a 1024 dimension shared state features extracted by PointNet++. The critic, sampler encoder, sampler decoder, and the policy network use PointNet++ architecture with 1024 dimension features to represent state s . The latents c in plan cVAE latent space \mathcal{C} has dimension 2 and is decoded into 64 dimension z_ϕ . Since the states in a trajectory are correlated, we replace all batch norms with group norms. We have experimented with sequence models for plan embedding but find a slower convergence.

The remaining timestep $(T - t)$ is concatenated feature-wise for the critic and the low-level policy and channel-wise for sampler networks to provide information about the horizon. Since the reward is bounded between -1 and 1 , we apply \tanh to the critic output heads and use the huber loss for the Bellman errors. The GA-DDPG option prediction is added as an extra head to the critic that does not depend on the trajectory latent. The actor network and the critic network are both implemented by a multi-layer perceptron with three fully-connected layers using the ReLU activation function. We use Adam [54] as the optimizer for training and decrease the learning rate in a piece-wise step schedule. We have experimented with other design choices such as predicting collision distance or using late-fusion for robot joints and do not observe performance improvement.

6.1.4 Training Details

Our offline training phase uses 120000 demonstration data points (around 2400 trajectories) from random scenes with ShapeNet objects. We use beta-cVAE [43] with hyperparameter $\beta = 0.02$ to trade off regularizing informative latent space for diverse sampling and plan reconstruction loss. We do not update the policy network when computing trajectory losses for the sampler latent in Eq. 3. Similar to [6], we adopt the point matching loss function to jointly optimize translation and rotation:

$$L_{\text{POSE}}(\mathcal{T}_1, \mathcal{T}_2) = \frac{1}{|X_g|} \sum_{x \in X_g} \|\mathcal{T}_1(x) - \mathcal{T}_2(x)\|_1, \quad (5)$$

where $\mathcal{T}_1, \mathcal{T}_2 \in \mathbb{SE}(3)$, X_g denotes a set of pre-defined 3D points on the robot gripper, and L1 norm is used. The same pose loss applies to all action and goal predictions. We have experimented with jointly modelling the plan sampler as Gaussian and regularize with plan encoder [34, 16] but observe worse plan encoding performance and training stability.

The sampler network, the plan embedding network, and the low-level policy are trained on offline dataset and fixed during the HRL phase. We resample 8 trajectory latents with random probability 0.1 in training time. GA-DDPG policy switch is added in an annealing schedule and the random switch steps are sampled from a normal distribution for the remaining steps with mean 8 and standard deviation 3. During each iteration of the online training, we sample 18 parallel rollouts of the actor to collect experiences. We perform 50 training optimization steps during each rollout. We adopt Clipped Double Q-learning [55] in practice where the first target network is updated every iteration with a Polyak averaging of 0.999 and the second target network uses 3,000 update step delay [4]. The MDP discount factor for DQN is $\gamma = 0.99$. We have experimented with the common RL fine-tuning approach of training sampler and critic jointly with mixed offline and online data and observe that the multi-modal plan generation is affected.

6.2 Additional Discussion

6.2.1 Potential Improvement

The joint embedding and low-level policy training scheme can be used to incorporate diverse sources of offline demonstration data for longer horizon tasks. PointNet and PointNet++ are used as feature extractor but more customized network architecture that models the object relations might be helpful for obstacle avoidance. To capture very distinct modes of trajectories in cluttered scene, the training cluttered-scene generations can be customized such as adding new objects during rollout to learn reactive behaviors and goal changes. Furthermore, a specific training schedule and curriculum can be designed for training and fine-tuning embedding, sampler, and critic due to their correlations.

Thanks to the point cloud state representation and the observation-conditioned policy, the learning system is interpretable since the sampled latent can be rolled out up to full horizon from only the current observation, similar to the computation of the plan point cloud trajectory. This can be treated as model-based rollouts in a deterministic and noise-free robot dynamics model. Therefore, the method can be also treated as a model-free analogy of MPC systems that incorporate lookahead planning by reactively sampling and selecting plans. Specifically we use the point cloud from current timestep as input s_t for the policy. The policy outputs an action a_t which can be inversely applied to s_t as the input for next timestep, i.e. $s_{t+1} = \mathcal{T}_a^{-1}(s_t)$ where \mathcal{T}_a denotes the $\mathbb{SE}(3)$ transform of the control prediction. The action plan can be further combined with analytic methods or trajectory optimizer before execution. Similar to other deep model-based and value-based methods, our approach leverages the parallelism advantage of GPU. Although only a random shooting scheme is used for the effective 2-dimension latent space, we can use a more complex zeroth-order optimization such as CEM and MPPI to improve the test-time performance.

6.2.2 Limitation and Consideration

This work uses goal-auxiliary policy instead of the common goal-conditioned ones, which can be a strict requirement to generalize across objects and environments in the real world. For target-driven grasping, we require a segmentation of the target object from the rest of the environment that are treated as obstacles. Therefore, the assumption on segmentation does not become more strict than single-instance grasping. In practice, GA-DDPG plays a big role in grasping success. We observe that switching too early might result in small collisions during grasping alignment and we often use a combination of heuristics and learned classifier. Although the sim-to-real perception gap is not a main issue with point clouds, the method has limitations on the sim-to-real contact modeling gap. The domain gap in contact modeling makes grasping certain objects difficult. To improve these failure modes, we can either perform real-world finetuning or improve contacts in the physics simulator. Furthermore, the sensor information such as depth and segmentation is limited when the robot is very close to the target. Separately training a grasp closure prediction network or a network to evaluate grasp closure might improve the performance. Finally, at some hard collision instances that require fine-grained controls, for instance the hand camera or fingers slightly collide with obstacles next to the target, the planner can struggle with generating diverse-enough trajectories and the latent critic also has trouble picking best trajectory among samples. Our simulation metrics can also be rigorous as any collision counts as negative reward. In real-world table-top test setting [50, 3], small collisions are often tolerable and only objects falling down count as collision.